Quaternary interaction of cryospheric and oceanographic processes along the central-east Greenland margin

Lara F. Pérez[1]; Tove Nielsen[1]; Tine L. Rasmussen[2]; Monica Winsborrow[2]*

*[1] Geological Survey of Denmark and Greenland (GEUS), Geophysical Department, Øster Volgade 10, DK-1350 Copenhagen, Denmark (*lfp@geus.dk; tni@geus.dk)*

[2] Centre for Arctic Gas Hydrate, Environment and Climate & University of Tromsø (UiT) – The Arctic University of Norway, Department of Geosciences, N-9037 Tromsø, Norway (tine.rasmussen@uit.no; monica.winsborrow@uit.no)

The east Greenland margin has been influenced by oceanographic and cryospheric processes since the late Miocene, when the southwards flow of the East Greenland Current (EGC) initiated and ice sheets first advanced across the margin. However, the relative importance of these processes, and their influence on the sedimentation of the margin through time remains poorly understood. High-resolution single-channel seismic, chirp sub-bottom profiles and swath bathymetry data were acquired along the middle/lower slope and proximal basinal area off Liverpool Land, central-east Greenland margin. In this study, seismic-stratigraphic and morphological analyses have allowed us to distinguish between major sedimentary processes occurred during the Quaternary. The stratigraphic architecture reveals mass transport deposits (MTDs) related to glacially influenced down-slope sedimentation. These are intercalated with buried contourite systems associated with bottom-current controlling the along-slope sedimentation. The distribution of the MTDs suggests influence of two distinct ice stream systems. Initial phases of down-slope deposition during the early-middle

Quaternary appear to be related to distal deposition fed by an ice stream from the Scoresby Sund area in the south. Whilst shallow sedimentary processes, together with morphological analysis of the seafloor, show that the most recent activity of down-slope processes during latest Quaternary has occurred in the north, linked to an ice stream from the Kong Oscar Fjord area. These observations document a temporal shift in the relative dominance of the Scoresby Sund and Kong Oscar Fjord ice stream systems. The glacial influence on the margin has been interrupted by periods of stronger activity of along-slope bottom current flow, demonstrating that the EGC periodically controlled sedimentation on the continental margin.

Key-words

Central-east Greenland margin; Quaternary glacial evolution; glacigenic debris flow; Scoresby Sund trough-mouth-fan; Kong Oscar Fjord glacial system; oceanographic processes.

1. Introduction

Since the mid-Pliocene onset of large-scale Northern Hemisphere glaciation, the cryospheric and oceanographic evolution of Greenland is considered to have followed the glacial-interglacial cycles of the Quaternary (e.g. Sarnthein et al., 2009). The impact of the Greenland Ice Sheet on the adjacent continental margins has been addressed in several works (e.g. Larsen et al., 1994; Hubberten et al., 1995; Swift et al., 2007; Thiede et al., 2010; Nielsen and Kuijpers, 2013; Knutz et al., 2015; Laberg et al., 2017); in particular the evolution, at different scales, of the ice streams which flowed through the major fjords and cross-shelf troughs (e.g. Stein et al., 1993; Solheim et al., 1998; Evans et al., 2002; Ó Cofaigh et al., 2003; Berger and Jokat et al., 2009; Laberg et al., 2013). However, most of the regional work relating to the Greenland Ice Sheet history has focused on the late Quaternary (e.g. Stein et al., 1996; Håkansson et al., 2007; Thiede et al., 2010; Zhuravleva et al., 2017).

The Quaternary oceanographic evolution of the northern North Atlantic is generally understood (Fig. 1A), including the present oceanographic pattern of the Greenland Sea (e.g. Wolf and Thiede, 1991; Våge et al., 2013; Håvik et al., 2017). The vertical water-column structure of the Greenland Sea has experienced little variation over the Quaternary, despite the dramatic climatic shifts (Raymo et al., 2004). However, variations did occur in the northwards advection of oceanic heat, in the meltwater input from the Greenland Ice Sheet and in the inflow and outflow waters through the surrounding straits, which resulted in, among other effects, a drop in North Atlantic Deep Water (NADW) formation during the Last Glacial Maximum (LGM) (Marchitto et al., 2002; Raymo et al., 2004; Zachos et al., 2008; Zhuravleva et al., 2017).

Detailed investigation of the interaction between cryospheric and oceanographic changes and their effect on the sedimentary processes has primarily been carried out along the western (Nielsen and Kuijpers, 2013; Knutz et al., 2015) and southeastern (Clausen, 1998; Rasmussen et al., 2003) Greenland margins, but so far the central and northern East Greenland margins has not been investigated in detail. As a novelty, in this study, offshore geophysical datasets from the central-east Greenland margin have been used to investigate the influence of cryospheric and oceanographic events within the long-term sedimentary record of the Quaternary. In particular, glacial-related features have been mapped and analysed to elucidate the evolution of the Greenland Ice Sheet along the margin, and the imprints of repeated advance-retreat cycles of local ice streams on the stratigraphic architecture of the margin. In addition, current-related features have been identified and related to variations in the regional oceanographic pattern and its influence in the construction of the margin. Thus, the main aim of the study is to reveal the cryospheric-oceanographic interactions influencing the construction of the central-east Greenland margin.

2. Regional framework

The study area is located oceanwards of the continental shelf edge, in the slope and proximal basinal area off Liverpool Land on the central-east Greenland margin (Fig. 1). Although, the Liverpool Land margin constitutes a passive margin, uplift occurred more recently during the early Pliocene influencing the ice sheet behaviour (Japsen et al., 2014; Døssing et al., 2016). Glaciations have played an important role in the building of the margin. Several major ice streams have operated on the continental shelf, carving cross-shelf troughs and depositing large prograding wedges forming trough-mouth-fans (TMFs) (e.g. Berger and Jokat et al., 2009), both common elements in high latitude margins (e.g. Nielsen et al., 2005). The Greenland Ice Sheet history started during the Eocene/Oligocene with a succession of cooling events before a major intensification of glaciations during the Pliocene/Pleistocene (Larsen et al., 1994; Solheim et al., 1998; Tripati et al., 2008). Last major advances of the Greenland Ice Sheet across the eastern shelf occurred during the Saalian Glaciation (0.20-0.13 Ma) (Vanneste et al., 1995; Solheim et al., 1998; Hakånsson et al., 2007) and the LGM, from which the last ice-retreat began (Evans et al., 2002; ÒCofaigh et al., 2002, 2004). In addition to these large-scale glaciations, several local glaciations have been documented along the central-east Greenland margin, such as the Scoresby Sund glaciation from 0.24 to 0.13 Ma and the Flakkerhuk glaciation from 0.06 to 0.01 Ma (Funder et al., 1994, 1998).

The present-day oceanographic pattern of the study area is dominated by the southwards flow of the East Greenland Current (EGC) (e.g. Våge et al., 2013). The evolution of this current has mainly been determined by the tectonic formation of the Fram and Denmark Straits (Fig. 1A). The Fram Strait represents the main connection between the Arctic Ocean and the Greenland Sea, whereas the Denmark Strait connects the Greenland Sea with the North Atlantic (Fig. 1A). The exact timing of the opening of the Fram Strait, as well as the generation of the deep-water oceanic connection, remains unresolved. Proposed opening time ranges from the Oligocene to the Miocene/Pliocene boundary (e.g. Engen et al., 2008; Ehlers and Jokat, 2013; Mattingsdal et al., 2014). The overflow of deep water from the Greenland Sea (mainly formed by Northern Component Water) through the Denmark Strait began during the early Miocene (Wright and Miller, 1996; Engen et al., 2008; Ehlers and Jokat, 2013), but it may periodically have been restricted by tectonic pulses along the Greenland-Scotland Ridge (Wright and Miller, 1996; Poore et al., 2006; Parnell-Turner et al., 2015). The onset of the flow of the EGC along the east Greenland margin is suggested to have occurred around 8.3 Ma (Wolf and Thiede, 1991; Våge et al., 2013). Since then, the flow of the EGC has been influenced by the glacial-interglacial fluctuations, which changed the position of the

Arctic Front and, as a consequence, the areal distribution of the water masses involved in the flow (e.g. Mokeddem and McManus, 2016). Thus, during southward advances of the Arctic Front, convection increases enhancing polar heat transport and favouring northern ice sheets growth (e.g. Mokeddem and McManus, 2016). At present, the EGC flow off Liverpool Land comprises several water masses occupying distinct depths in the water column. The Polar Water occupies the continental shelf shallower than 200 m (Aagaard and Coachman, 1968); the Return Atlantic Current (RAC) carries Atlantic Intermediate Water between 150 and 800 m (Hopkins, 1991); whilst the lower continental slope and basinal area are influenced by the Greenland Sea Deep Water (GSDW), generated by convection in the Greenland Sea (Hopkins, 1991; Jeansson et al., 2008).

3. Data and methods

3.1 Database

The dataset used in this work consists of swath bathymetry, chirp sub-bottom profiles and high-resolution single-channel seismic data (Fig. 1B). The data were obtained in 2013 onboard the *R/V Helmer Hanssen* led by the Department of Geosciences at University of Tromsø (UiT) – the Arctic University of Norway – and the Centre for Arctic Gas Hydrates, Environment and Climate (CAGE). The swath bathymetry was acquired with a Kongsberg Maritime EM300 multi-beam and EK60 split-beam (18, 38 and 120 kHz) echo sounders covering both deep and shallow water depths over an area of 1500 km^2. Sound velocity profiles of the water column were acquired for calibration. Preliminary processing of the multi-beam data was performed using Neptune software, while post-processing was done with Fledermaus software. DMagic software was used to generate grids with 30 m cell-size. Visualization and interpretation of these data were carried out using Fledermaus and ArcGIS software. Chirp sub-bottom profiles, with a total length of 1004 km, were obtained simultaneously with the multi-beam data (Fig. 1B). The acquisition system was a hull-mounted EdgeTech 3300-HM sub-bottom profiler operating at 3.5 kHz. Pulse mode and shot rate were varied depending on the water depth. The maximum penetration is 35-40 ms two-way-travel-time (TWTT) and was obtained in the southern part of the study area.

Four high-resolution single-channel seismic profiles, with a total length of 155 km were acquired on the lower slope, and at the base of the slope within the study area (Fig. 1B). The seismic source was a single Sercel GI mini airgun of 45 cubic inches and the receiver was a single-channel steamer of 6 m active section with 20 hydrophones. The sampling rate was 0.5 ms. Post-processing of the seismic data followed a normal sequence of single-channel processing. The seismic penetration allows a detailed analysis down to 0.4 s TWTT below the seafloor and identification of major seismic features to about 1 s TWTT below the seafloor. Interpretation of the sub-bottom and seismic profiles was carried out using Petrel software, following conventional seismic stratigraphic analysis (e.g. Payton, 1977).

3.2 Age estimation

The age model of the major seismic units identified in the present study is adapted from a newly established stratigraphic framework for the central-east Greenland margin (Pérez et al., 2018). This work presents a reconstruction of the central-east Greenland margin since Miocene times, providing an estimated age of the mapped stratigraphic discontinuities by correlation with Site 987 of ODP Leg 162 located in the basinal area off Scoresby Sund (Jansen et al., 1996; Channell et al., 1999; Pérez et al., 2018). The ODP 987 region is connected to the central-east Greenland margin by a network of seismic profiles (Fig. 1B). A comparison of the large-scale seismic patterns of these seismic lines with those of the present study, allows correlation of the two upper units of the stratigraphic model presented in Perez et al. (2017) to the seismic network of this work as shown in Fig. 2. Thus, according to the chronological model, the age of the lower seismic unit of the present work, seismic unit U2 (see below), is assigned to the middle Pleistocene. The base of U2 is formed by a regional stratigraphic discontinuity Discontinuity-b of an estimated age of 2.05 Ma (Pérez et al., 2018). The age of the upper seismic unit of the present study, seismic unit U1 (see below), is assigned to the late Pleistocene-Holocene. The top of U1 is defined by the seafloor and therefore considered as 0 Ma, and the base of the unit is formed by the seismic Discontinuity-a of Pérez et al. (2018) (Fig. 2, 3). The age of Discontinuity-a was estimated to 1.6 Ma and thus correlates to the age of seismic reflector R1 of earlier chronostratigraphic models of the ODP site 987 (Jansen et al., 1996; Channell et al., 1999). In the present study, U1 was divided into subunits (see below), which could also be recognised, based on affinity of seismic facies, on two seismic profiles of the former study area (GGUi82-12 and 11HH-GEO8144-022; Fig. 1B) and could thus be tied to ODP 987 for an approximate age estimation using linear interpolation (Jansen et al., 1996; Butt et al., 2001; Laberg et al., 2013; Perez et al., 2017) (Fig. 3).

During the 2013-expedition several gravity and piston cores were recovered in the study area (Fig. 1B). Gravity core HH13-099GC is located over line CAGE-OA2013-034, recovering 5.41 m of sediments at 1550 m water depth. The average sound velocity in the sediments is 1579.17 m/s measured in the core (Rasmussen, *unpublished data*). The magnetic susceptibility profile of this core is similar to the curves of gravity cores HH13-093GC and HH13-092GC located in the basinal area to the SE of the study area (Fig. 1B, 4). Core HH13-092GC recovered 3.1 m of sediments at 1595 m water depth that have been AMS ^{14}C dated, calibrated to calendar years and correlated to isotope

201 stages (Fig. 4). An age of 46.8 cal ka is found at 2.05 m below the seafloor (Fig. 4). These ages are in agreement with those previously published by Stein et al. (1996) off central-east Greenland margin. Using the dating from these gravity cores (Fig. 1B, 4), and assuming a relatively steady sedimentation rate in the study area during the late Quaternary, the age of the base of the upper subunit can be estimated to *ca.* 0.4 Ma, which agrees with the age estimated for this horizon from ODP 987 (Fig. 3, 4).

3.3 Terminology

The morpho-sedimentary nomenclature used in this paper is clarified below. 'Contourites' refers to sediments deposited or substantially reworked by the persistent action of bottom currents (e.g. Stow et al., 2002; Rebesco, 2005). This term thus includes a large array of sediments affected to varying degrees by different types of currents (Rebesco et al., 2014). Thick, extensive sedimentary accumulations are considered 'contourite drifts' or 'drifts'. We adopted the contourite drift classification criteria from Faugères et al. (1999) and Rebesco (2005) identifying two main types of drifts: (i) the mounded drifts, which are mounded and elongated; and (ii) the sheeted drifts, which are represented by broad, tabular to slightly mounded geometries. A third type, usually called plastered drifts, has a morphology that lies between the two other types (e.g. Rebesco et al., 2014). Sediment waves are frequently associated with contourite drifts, expressed as transverse, asymmetric bedforms of smaller dimensions. The crests of contourite-related sediment waves are slightly sinuous, with rare bifurcation and aligned perpendicular or oblique to the flow direction (Wynn and Stow, 2002). Contourite-related sediment waves represent deposition under long-term stable current conditions at low flow-velocities (Stow et al., 2002; Rebesco et al., 2014). In contrast, sediment waves related to across-slope flows present moderate sinuosity and regular bifurcation and are commonly found parallel to the slope or rise between channels or sedimentary lobes (Wynn and Stow, 2002).

Mass transport deposits (MTDs) have been identified as bodies having internal seismic facies similar to that described by Reading (1996) as transparent or semi-transparent seismic facies in which internal reflections may be locally observed. Among the large variety of MTDs, glacigenic debris-flow (GDF) deposits are acoustically transparent or semi-transparent bodies, that lack the chaotic and higher amplitude acoustic character of the larger slope failures such as sediment slides (Pickering and Hiscott, 2016). The term 'GDF system' is used in this work for the combination of MTDs and channel-levees of glacial origin (e.g. Laberg and Vorren, 1995). Considering the vertical resolution of the seismic data (~ 3 m), individual MTDs could comprise several events undistinguishable at the seismic scale, and therefore, they could be considered as mass transport complexes as defined by Pickering and Hiscott (2016).

Pockmarks are nearly circular depressions formed where fluids escape through the seafloor sediment (Cathles et al., 2010). These imprints are common where gas is present in the near seafloor sediments and are usually associated with other fluid migration structures such as chimneys or polygonal faults (Cathles et al., 2010). Pockmarks and fluid migration structures are identified in this work and mentioned as part of the margin description, but otherwise not further discussed.

4. Results and interpretation

4.1 Physiography

The study area is located off northern Liverpool Land where the continental shelf widens from 70 to 100 km from south to north (Fig. 1B). The wide continental shelf is generally over 200 m deep, deepening to 400 m at the shelf edge. It presents an irregular morphology marked by several cross-shelf troughs. The slope, about 30 km wide, passes into the basinal area of the southern and shallowest part of the Greenland Sea with water depths over 1700 m (Fig. 1B).

The upper slope extends from 400 to 700 m water depth with gradients between 5^o and 3^o, being wider and gentler in the north. The swath bathymetry data extends from the middle slope to the adjacent basinal area where the depth varies between 650 and 1770 m below sea level (Fig. 1B, 5). The middle slope is characterised by gradients ranging from 4^o in the south to 2^o in the north, whilst the lower slope is gentler with gradients of 2^o in the south and 1^o in the north. The middle and lower slopes show a relatively smooth surface morphology in the south whereas they have an irregular morphology in the northern area (Fig. 5). The base of the slope is located more proximal in the south relative to the north of the study area. The gradient of the basinal area is 0.3^o-0.2^o and it has a smooth morphology, particularly in the northern part (Fig. 5).

4.2 Seafloor morphological features

Several incisions are identified across the middle slope, particularly in the northern part of the study area. These are referred to as middle-slope channels and trend 30^{o}ESE (Fig. 5). The middle-slope channels display a V-shaped cross-section about 200 km wide and 2 m deep, reaching water depths of nearly 1580 m. Larger incisions, also V-shaped and with the same orientation, are identified across the northern part of the lower slope. These are referred to as lower-slope channels. The largest are 200 to 700 m wide and about 5 m deep (Fig. 5). They run over a distance of 3000 to 8000 m, ending in water depths of 1650 m. Both the middle- and lower-slope channels have an erosive character and are interpreted to have been formed by downslope flows related to mass transport of sediments. Some other incisions are identified in the southern basinal area.

These incisions are 350 m wide and 1.5 m deep and run over a distance of 2 km between water depths of 1658 and 1665 m (Fig. 5). They are interpreted to be distal channels, representing the most-oceanwards extent of downslope flows and connected to distal transport of sediments.

Two of the lower-slope channels end in small monticules (300 m across slope x 1000 m along slope) that stretch parallel to the slope, but generally the channels are located adjacent to vast lobe morphologies perpendicular to the margin at the base of the slope. The depositional lobes are particularly well-developed in the northern part of the study area where two major lobes are identified at the base of the slope (Fig. 5): the northern lobe is 3014 m wide and 3760 m long, whereas the southern lobe is 2160 m wide and 3110 m long (Fig. 5). Both depositional features, i.e. monticules and lobes, are interpreted to be associated with the deposition of sediments from downslope mass transport. Considering the glacial nature of the study area, the erosive channels and depositional features are interpreted as part of GDF systems.

Round-shaped depressions are identified on the southern lower slope. They show a U-shaped profile of about 200 m wide and 5 m deep, and are concentrated in water depths of about 1500 m (Fig. 5). These depressions are interpreted as pockmarks according to Cathles et al. (2010) and related to fluid and/or gas escape at the seabed, following migration through the sedimentary record.

Undulating seabed morphologies are identified at the base of the slope in the northern part of the study area and in the proximal basinal area (Fig. 5A). They are interpreted as sediment waves. The largest waves are 230 m wide and 4 m high, and sinuously extend over 2 km (Fig. 5). They are roughly parallel to the slope and located between the lower-slope channels and the depositional lobes. These sediment waves are interpreted as related to an across-slope flow in agreement with the discrimination of

Wynn and Stow (2002). In the proximal basinal area, the sediment waves are less pronounced, about 100 m wide and 1 m high and with straight or slightly sinuous crests. They are oblique to the margin and particularly abundant along the southern part of the study area, where the largest ones extend about 3 km (Fig. 5). These sediment waves are interpreted to be related to the mobilisation of sediments by along-slope currents according to Wynn and Stow (2002) and the classification of Stow et al. (2002).

4.3 Shallow sub-bottom features

Different acoustic facies are distinguished on the chirp sub-bottom profiles (Fig. 6). The middle and lower slope is generally characterised by low-penetrative facies, with an irregular seafloor reflection and few-to-no sub-bottom reflections (Fig. 7A, 8A). We interpret these facies to be associated with MTDs (see section 3.3) and formed by sediments running downslope from the continental shelf. The identified MTDs have a relatively transparent acoustic response and therefore they are interpreted as GDF deposits, formed by sediment instability generated by the oceanward advance of the ice sheet over the continental shelf.

The base of the northern slope is characterized by internal chaotic facies overlain by subparallel reflections with a wavy-irregular seafloor expression, defined as ridge and valley topography (Fig. 6, 7A, 8A), following the morphological nomenclature of García et al. (2012). Oceanwards, stratified and laterally continuous reflections are slightly tilted, forming a laminated body at about 1700 m water depth (Fig. 6). The laminated body is interpreted as a plastered contourite drift, according to the classification established by Faugères et al. (1999) and Rebesco (2005). In the basinal area the plastered drift onlap onto lateral continuous, undulating reflections that form a mounded body between 1725 and 1740 m water depth (Fig. 6). This body is interpreted to be a mounded contourite drift based on Faugères et al. (1999) classification.

The proximal area of the plastered drift displays an irregular surface over sub-bottom vertical structures (Fig. 6). Farther south, at the base of the slope, a similar pattern with horizontal and stratified reflections disrupted by scattered vertical fractures and underlain by MTDs is identified (Fig. 8A). These structures are interpreted to have formed due to the migration of fluids through the upper sedimentary record.

The southern base of the slope and basinal area is characterized by a generally stratified sub-bottom pattern of laterally continuous reflections that are slightly undulating (Fig. 6B, 7A, 8A). Locally small transparent bodies with lenticular shapes (~800 m length and ~4 ms TWTT thick), considered to be small MTDs, are identified both on the seafloor and deeper in the stratified sedimentary record (Fig. 6, 7A, 8A). Two pronounced acoustic reflections, together with a strong reflectivity variation, allow us to define three chirp units in the shallow sub-seabed section (Fig. 7A, 8A). The lower chirp unit (c3) is characterised by high reflectivity that decreases downwards. The base of c3 is not visible on the sub-bottom profiles. The middle chirp unit (c2) is characterised by low reflectivity (Fig. 7A, 8A), and its thickness increases to the southwest with a maximum along the proximal basinal area in the central and southern part of the study area (more than 20 ms TWTT thick; Fig. 5B). The upper chirp unit (c1) has high internal reflectivity and a maximum thickness (more than 20 ms TWTT) along the base of the slope in the central study area, thinning to the south (Fig. 6B, 7A, 8A).

4.4 Seismic-stratigraphy

Seismic-stratigraphic analysis of the high-resolution seismic profiles allows us to distinguish major stratigraphic unconformities from the present seafloor down to 2.7 s TWTT depth (Fig. 7B, 8B). Following the regional stratigraphic model published in

Pérez et al. (2018), the sedimentary record is divided into two major seismic units (U2 and U1 from bottom to top) that are separated by a major regional unconformity called Discontinuity-a (Fig. 2). The seismic resolution of the lower seismic unit U2 is very low forming a relatively homogeneous layer with few internal reflections; although to the north of the study area, reflections of low lateral continuity can be identified in its upper part (Fig. 7B, 8B). The thickness of U2 varies from 285 ms TWTT along the northern lower slope to 200 ms TWTT along the base of the slope (Fig. 9A).

The distribution of the overlying seismic unit U1 is more heterogeneous, compared with U2. The thickness of the unit decreases southeastwards from 410 ms TWTT on the northern lower slope to 150 ms TWTT in the southern proximal basinal area, although the maximum thickness of 490 ms TWTT is located on the southern middle slope (Fig. 9A). The seismic resolution of U1 allows us to identify several stratigraphic features and to divide the unit into five minor subunits based on seismic facies variations. The subunits are named SU5 to SU1 from bottom to top, and are bounded by less distinct stratigraphic discontinuities that locally represent unconformities (Fig. 7B, 8B).

The lowermost subunit (SU5) increases in thickness downslope, from 32 ms TWTT along the lower slope to 100 ms TWTT at the base of the slope (Fig. 9B). Internal reflections within this subunit have relatively high lateral continuity and are organized in a stratified pattern (Fig. 8B). The stratified pattern is locally interrupted by vertical structures that indicate fluid migration through SU5 (Fig. 7B). Along the middle and lower slope the stratification is also interrupted by several zones of chaotic facies. These chaotic zones are formed by a strong erosion —marked by erosive truncation of the reflections— that laterally continues into wavy reflections with low lateral continuity forming mound-shape bodies (Fig. 7B). These morphologies are interpreted to represent channel-levee complexes usually associated with turbidity currents (e.g. Mulder et al., 2008; Nelson et al., 2011). Along the southern base of the slope and basinal area the stratified pattern is replaced by sedimentary bodies with transparent to semi-transparent seismic signatures interpreted as MTDs (Fig. 7B, 8B). The maximum thickness of these bodies is 44.2 ms TWTT, located in the southeast basinal area (Fig. 8B). The combination of turbidity current-related features and MTDs are associated with GDF systems. However, in the southern part of the basinal area an erosive U-shaped zone continues laterally in a slightly mounded body, which is interpreted as a buried drift-moat system.

Above, subunit SU4 forms a thin layer the thickness which decreases from 62 ms TWTT along the lower slope to 22 ms TWTT in the southeastern base of the slope area (Fig. 9B). Internal reflections have a low lateral continuity and an undulating morphology, indicating sediment waves (Fig. 7B, 8B). Several erosive areas marked by erosive truncations are identified inside this subunit, particularly along the base of the slope (Fig. 8B). As within SU5, the reflection pattern of SU4 is also interrupted by MTDs. In the lower part of the unit they are interbedded within the generally stratified reflection pattern; however, widespread MTDs dominate the upper part of SU4 (Fig. 7B, 8B). The maximum thickness of the MTDs is 50 ms TWTT. The stratified reflections at the northern base of the slope form a mounded body with northward progradation of the reflections, which resemble the morphology of a buried laminated or plastered drift (Fig. 8B).

Subunit SU3 has a maximum thickness along the northern lower slope (92 ms TWTT) (Fig. 9B), thinning towards the south (27 ms TWTT) and east, and disappearing in the northern base of the slope. Internally, this unit is represented by mostly transparent to semi-transparent facies with some areas of high amplitude reflections, laterally discontinuous in the central part of the study area (Fig. 7B, 8B). MTDs are identified in particular along the northern lower slope where their thickness reaches 90 ms TWTT (Fig. 7B).

Subunit SU2 has highly variable thickness. It is thickest along the middle and lower slope, where it reaches 250 ms TWTT in the south and 151 ms TWTT in the north (Fig. 9B). Along the base of the slope it is only identified in the northern part, where its thickness reaches 76 ms TWTT. Internally SU2 comprises several large MTDs of highly variable thickness. These are bounded by a few high amplitude reflections with low lateral continuity (Fig. 7B, 8B).

Subunit SU1 forms a thin upper layer. Its thickness increases from 20 to 200 ms TWTT on the central and northern lower slope respectively (Fig. 9B), whereas it is more uniform along the base of the slope (over 40 ms TWTT). In the south, it presents a stratified pattern with slightly undulated, relatively lateral continuous internal reflections. Several MTDs disrupt the stratified pattern of the unit in the northern lower slope (Fig. 7B, 8B). The thickness of the MTDs is about 40 ms TWTT. Vertical fractures and sediment mobilisation features associated with fluids migration can be identified along the base of the slope (Fig. 7B).

5. Discussion

Most sedimentary processes identified off Liverpool Land, based on the results of this study, are observed within seismic unit U1, i.e. between the Discontinuity-a and the seafloor (Fig. 7B, 8B). According to previously proposed stratigraphic models (see section 3.2) and the regional stratigraphic correlation (Fig. 2), this unit encompasses the Quaternary stratigraphic record from 1.6 Ma to the Present (Fig. 3). In agreement, the underlying seismic unit U2 potentially represents the early Quaternary period (2.05 - 1.6 Ma). Within the study area, the U1 sediment thickness increases northwards in contrast with the U2 sediment thickness that increases southwards, indicating an overall change in the sediment distribution during Quaternary (Fig. 9B), which is interpreted to be related to a change in the prevalent sediment source. The sediments are mainly delivered from the southern part of Liverpool Land during early Quaternary and from the northern part of Liverpool Land during late Quaternary.

5.1 Cryospheric influence on the sedimentary processes

North of our study area, and associated with the Kejser Franz Joseph fjord, four main phases of Quaternary GDF systems formation have been identified previous to this work (Wilken and Mienert, 2006). Despite a common formation process, the GDF systems off Liverpool Land have a stratigraphic distribution that differs from those described in the Kejser Franz Joseph fjord area, as discussed below.

In the lowermost identified seismic subunit off Liverpool Land, SU5 (early Pleistocene age), the buried turbiditic-channel systems along the lower slope (Fig. 7B), led to the formation of buried GDF deposits at the base of the slope predominantly observed in the southern part of the study area. This configuration points to a distal downslope input from a glacial system in the Scoresby Sund area (Fig. 7B, 8B, 9). The resulting GDF systems off Liverpool Land are related to ice streams flowing along the Scoresby Sund fjord and crossing the continental shelf; a scenario that is consistent with the high sedimentation rates, dropstones and sandy turbidities identified in ODP 987 (Jansen et al., 1996) and the large sediment input to the northern part of the Scoresby Sund TMF between 1.77 and 0.78 Ma (Laberg et al., 2013). The formation of the GDF systems identified in SU5 off Liverpool Land must have been triggered by grounded ice located on the outer shelf or at the shelf edge off Scoresby Sund. This is in contrast to the early Pleistocene system north of Kejser Franz Joseph fjord described by Wilken and Mienert (2006), where the sedimentary record is characterised by an extensive deep-sea channel system and proximal formation of GDF deposits formed by an ice sheet located landwards from the shelf edge. The reduced extension of the ice sheet off Kejser Franz Joseph fjord occurred during relatively warm conditions (Zhuravleva et al., 2017). The differences between the offshore sedimentary systems of Scoresby Sund and Kejser Franz Joseph during early Pleistocene indicate a sedimentation pattern that suggests that the Greenland Ice Sheet extended farther across the continental shelf in the Scoresby Sund area compared to the northern East Greenland fjords (Fig. 10).

The number of GDF deposits off Liverpool Land increased during SU4 sedimentation in the mid-Pleistocene (Fig. 3, 7B, 8B). We speculate that this upwards increase in GDF deposits occurred in line with the increase in global ice volume that accompanied the mid-Pleistocene transition (also known as mid-Pleistocene revolution) (Head and Gibbard, 2005; Laberg et al., 2017). This climatic shift took place between 0.9 and 0.92 Ma and represents the onset of the high amplitude 100-ka Milankovitch cycles, when precession-driven variations became more important (Berger and Wefer, 1992; Raymo et al., 1997). The GDF deposits found in the southern part of subunit SU4 indicate an enhanced sedimentary input to the northern part of the Scoresby Sund TMF prior to 0.78 Ma. Some GDF deposits are also identified within SU4 in the northern part of the study area, pointing to the inception of an important ice stream through the northern fjord, i.e. Kong Oscar Fjord (Fig. 10). This change in the glacial stage of the central-east Greenland during the mid-Pleistocene is also reflected in the significant change of the sedimentary pattern that occurred off Liverpool Land where the primary depocentres migrated landwards to the northern lower slope during this period (Fig. 7B, 8B, 9B). The northern glacial advance could have caused the decrease in the input of meltwater from the Greenland Ice Sheet to the east margin (Zhuravleva et al., 2017).

The extension of the ice sheet to the northern Liverpool Land occurred at the time of the first identified GDF deposits on the North Sea Fan (1.1 Ma; Nygard et al., 2002) suggesting a regional increase in the activity of ice streams around the North Atlantic.

The two overlying subunits, SU3 and SU2, are mainly formed by large MTDs marking a dominant downslope control on sedimentation off Liverpool Land (Fig. 7B, 8B). We associate this downslope deposition with the glacial intensification at 0.8 Ma, in agreement with grounded ice extending across the margin ─tentatively to the shelf edge─ that launched ice rafting of sediments eroded from the shelf and the formation of GDF deposits through sediment transport across the continental shelf and down the slope (Alley et al., 1989; Berger and Jansen, 1994; Dowdeswell et al., 1997; Bart et al., 2000; Stokes et al., 2016; Laberg et al., 2017). Farther north of the study area, MTDs have likewise been related to full-glacial conditions and early stages of deglaciation (García et al., 2012). The internal distribution of the GDF deposits within SU3 and SU2 points to a changing sediment source through time (Fig. 10). While the lowest lying GDF deposits are more abundant in the southern part off Liverpool Land, and thus may have been generated by a southern source, the upper lying GDF deposits are more abundant in the northern study area, indicating a northern sediment source (Fig. 10). This distribution of the GDF deposits suggests that the activity of the Scoresby Sund ice stream system decreased as the Kong Oscar Fjord ice stream system activity increased, indicating a northward advance of the east Greenland cross-shelf glaciation.

The youngest seismic subunit, SU1, indicates a major change in the sedimentary pattern off Liverpool Land that occurred at about 0.4 Ma, according to the estimated age of this subunit (Fig. 3, 4). The distribution of sediments, characterised by depocentres on the northern lower slope, and the southern stratified pattern of SU1 are taken as evidence of a lack of downslope transport processes from the Scoresby Sund ice stream system (Fig. 7B, 8B, 9B). This is in agreement with the ice-rafted debris (IRD) trapped in the Scoresby Sund fjord during the last 10 ka when only a minor amount of IRD reached the open shelf (Stein et al., 1993). However, the MTDs identified in the northern part of the study area indicate downslope processes across the lower slope (Fig. 7B, 8B). They may be related to advance of ice through Kong Oscar Fjord and across the continental shelf during the Saalian and Weichselian glacial periods (Hubberten et al., 1995). Farther north, moraines related to the maximum extent of the Greenland Ice Sheet during the LGM have also been identified on the mid-shelf off Kejser Franz Joseph Fjord (Evans et al., 2002). In addition, SU1 includes the period of maximum concentration of IRD in the upper continental slope in relation to the glaciation of the Jameson Land (Funder et al., 1998), when the ice sheet reached the mid-shelf (Funder et al., 1998; Evans et al., 2002); and the 0.2 Ma peak of GDF deposits along the east Greenland margin when the ice sheet last extended to the shelf edge (Wilken and Mienert, 2006).

In addition to the differences in sedimentary processes between the two zones within SU1 distinguished off Liverpool Land, there are also clear morphological differences distinguishable on the swath bathymetry data and sub-bottom profiles (Fig. 5, 6). Although having occurred within the last 0.4 Ma, there is no evidence of recent downslope transport across the lower slope in the southern part of the study area, as reflected in the stratified pattern of the chirp units (c1, c2 and c3) identified in the southern basinal area (Fig. 6B), i.e. at the northern Scorceby Sund TMF (Fig. 11), which is in accordance with observations by O’Cofaigh et al., (2002). The differences in the downslope sediment transport activity off Liverpool Land may relate to the slightly steeper slope in the south compared with the northern part of the study area, which would support longer run-out distances oceanwards in the south. Thus, the gradient of the southern lower slope eases reworking of the MTDs into turbidity currents, evidenced by the distal channels in the basinal area (Fig. 5) and resulting in an effective by-passing across the slope (Pudsey and Camerlenghi, 1998; O'Cofaigh et al., 2003). In contrast, the channels, monticules and depositional lobes that form the GDF systems observed in the northern part of the study area, provide evidence of downslope sediment transport processes controlling the sedimentation and morphology of the middle and lower slopes (Fig. 5, 6, 11), as occurred during the SU1 formation. This difference could denote a recent larger sediment input, or slope instability, in the northern part compared to the southern part of the study area as discussed for SU1. The depocentres of the chirp units c2 and c1 reflect a northward migration, as occurred in the general trend on the discussed seismic units and subunits, supporting a northward relocation of the main sediment source along the Liverpool Land margin. However, the physiography of the slope is important since it determines the post-failure behaviour of the displaced sediments (Migeon et al., 2011). The gentle slope in the northern study area, where the continental shelf is also wider, makes it closer to the conceptual model of a classic TMF system (e.g. Polar North Atlantic; Dowdeswell et al., 1997; King et al., 1996, 1998; Vorren and Laberg, 1997) where the fan formation occurred during glacial maxima (O'Cofaigh et al., 2003). In this case, the seafloor GDF systems observed off Liverpool Land may be related to the glaciations known as Scoresby Sund and Flakkerhuk (Funder et al., 1994, 1998), as are the depositional lobes described north of Kejser Franz Joseph fjord (Wilken and Miernert, 2006). In agreement with the GDF systems formed off Liverpool Land during the Quaternary, and discussed in the previous section, the TMFs would reach their maximum growth in the northern part of the study area during the maximum oceanwards location of the grounded ice sheet, whereas the morphology of the southern slope would favour a distal transport of sediments during ice sheet stability periods.

5.2 Oceanographic influence on the sedimentary processes

A variety of current-related deposits, i.e. different kind of drifts and sediment waves, has been identified particularly along the base of slope and proximal basinal area off Liverpool Land. These current-related features are common at the seafloor and within the Quaternary sedimentary record, intercalated with the GDF systems. They may have been locally masked or eroded by other dominant processes, e.g. in SU3 and SU2 where the observed downslope sedimentation may have removed potential current-related features (Fig. 7B, 8B). The identified current-related features vary from drifts to wavy facies indicating action, to various degrees, of bottom currents over the seafloor at the time of deposition (Stow et al., 2002). The coexistence of current-related and glacial-related deposits identified in the geophysical data in this work reveal a cryospheric-oceanographic interaction in the construction of the central-east Greenland margin.

A buried drift-moat system is identified in the SU5 in the southern basinal area of the study area indicating active along-slope bottom currents during the formation of the subunit. Based on location and morphology (Fig. 8B), the system is interpreted to have been deposited by a bottom current similar to the present anti-clockwise flow of the GSDW in the southern Greenland Sea (Jeansson et al., 2008). Thus, formation of this drift-moat system is suggested to involve GSDW convection in the Greenland Sea basinal area off Liverpool Land during middle Pleistocene.

The presence of sediment waves and buried drifts observed at the base and lower slope slightly north in the study area within SU4 suggests an active bottom water flowing southwards along the slope (Fig. 7B, 8B). The change in the character and location of the drifts from SU5 to SU4 suggests an apparent increase in along-slope current-related deposits, which could relate to the shift from intense, but zonal, oceanic circulation at high latitudes prior to the mid-Pleistocene transition, to meridional deep water flows and major water mass exchange with the North Atlantic, starting a strong overflow of bottom water from the Greenland Sea to the North Atlantic (Berger and Jansen, 1994; Baumann and Huber, 1999; Helmke et al., 2005). Even though there was a suppression of formation of NADW in the Greenland Sea during the mid-Pleistocene, this occurred together with an increased warm water advection and vigorous influx of oceanic heat to the Greenland Sea due to the progressive northward migration of the Arctic Front (Berger and Jansen, 1994; Raymo et al., 1997; Henrich et al., 2002; Wright and Flower, 2002).

The distribution and configuration of SU1 off Liverpool Land seems determined by the irregular morphology of the underlying unit. However, the undulating reflections observed along the southern lower slope and proximal basinal area suggest a slight influence of bottom current activity (Fig. 7B). It is also supported by the slightly undulated signature of the reflections, which form the recent chirp units, c1, c2 and c3 (Fig. 7B). The influence of bottom current in these areas is also revealed by the contourite drifts identified in the sub-bottom sedimentary records and the contourite-related sediment waves in the seafloor morphology. The late Pleistocene onset of this bottom current activity is in agreement with the reported increase in strength of glacial-related NADW formation from 0.4 Ma, even though the reasons for the increased production of NADW remain unclear (Raymo et al., 1997). The components of NADW did not vary significantly on glacial-interglacial timescales for most of the Pleistocene, thus deep-water formation north of the Denmark Strait continued although its production decreased during the LGM (Marchitto et al., 2002, Raymo et al., 2004).

The sediment waves identified at the southern lower slope and proximal basinal area off Liverpool Land are interpreted to be related to the activity of along-slope flows during the recent past and present margin history based on their morphology and distribution with respect to the margin (Fig. 5). However, the sediment waves identified at the base of the slope in the northern part of the study area are interpreted as turbidity-related features in agreement with the interpretation of the sediment waves off the northeast Greenland margin (Garcia et al., 2012). Contourite drifts are identified in the shallow sub-bottom and seafloor records, particularly in the northern basinal area (Fig. 6). Both types of current-related deposits, i.e. sediment waves and contourite drifts, off Liverpool Land reveal relatively intense activity of along-slope bottom currents (Fig. 11). These bottom currents must be related to the EGC flowing southwards along the margin, but in the depth-domain of the GSDW. The observed differences of these features between the northern and southern parts off Liverpool Land could be associated with a vertical mixture of the GSDW with the above-flowing RAC (Jeansson et al., 2008), which would generate variations within the flow.

6. Conclusions

The sedimentary processes observed along the slope off Liverpool Land reveal interaction between oceanographic and cryospheric processes in the construction of the margin during the Quaternary. While the oceanographic processes are mainly related to the southwards flow of the East Greenland Current and the formation of the Greenland Sea Deep Water within the Greenland Sea, the glacial influence on the margin is marked by the interaction between the various ice streams that originated from the main fjord systems of central-east Greenland. The southern ice stream associated with the Scoresby Sund glacial system was most active during the Pliocene and early-middle

Pleistocene, however from the middle Pleistocene to the present-day most of the downslope sediment transport to the basinal area is related to the northern Kong Oscar Fjord glacial system. The abundance of Glacial Debris Flow deposits between 0.8 and 0.4 Ma points to ice streams reaching the shelf edge off Liverpool Land, whereas the northern ice streams reached the shelf edge off Kejser Franz Joseph fjord only during the last 0.15 Ma according to Wilken and Mienert (2006). This northwards migration in the formation of glacigenic debris-flow systems and the oceanward ice-edge position confirm the northward migration of the glaciation along the central-east Greenland margin since the early Pleistocene.

Acknowledgements

The research developed for this work has doing under the GLANAM (GLAciated North Atlantic Margins) Initial Training Network FP7/2007-2013/ under REA grant agreement n° 317217. We thank the Department of Geosciences at University of Tromsø (UiT) – the Arctic University of Norway – and Centre for Arctic Gas Hydrates, Environment and Climate (CAGE) for the personal and technical support during the initial development of the research, in particular Professor Karin Andreassen. T. L. Rasmussen and M. Winsborrow were supported by the Research Council of Norway through its Centres of Excellence funding scheme, project number 223259. We acknowledge the suggestions of Dr. Dove and Dr. García that helped to improve the first version of the manuscript.

References

Aagaard, K., Coachman, L. K. & Institute of North America 21, N. 1968: The East Greenland Current II. ARCTIC, *Journal of the Arctic Institute of North America* 21, 267-290.

Alley, R. B., Blankenship, D. D., Rooney, S. T. & Bentley, C. R. 1989: Sedimentation beneath ice shelves - the view from ice stream B. *Marine Geology* 85, 101-120.

Bart, P. J., Anderson, J. B., Trincardi, F. & Shipp, S. S. 2000: Seismic data from the Northern basin, Ross Sea, record extreme expansions of the East Antarctic Ice Sheet during the late Neogene. *Marine Geology* 166, 31-50.

Baumann, K. H. & Huber, R. 1999: Sea-surface gradients between the North Atlantic and the Norwegian Sea during the last 3.1 m.y.: Comparison of Sites 982 and 985. *Proceedings of the Ocean Drilling Program: Scientific Results* 162, 179-190.

Berger, D. & Jokat, W. 2009: Sediment deposition in the northern basins of the North Atlantic and characteristic variations in shelf sedimentation along the East Greenland margin. *Marine and Petroleum Geology* 26, 1321-1337.

Berger, W. H. & Jansen, E. 1994: Mid-Pleistocene Climate Shift - The Nansen Connection. The Polar Oceans and Their Role in Shaping the Global Environment, 295-311 pp. *American Geophysical Union*.

Berger, W. H. & Wefer, G. 1992: Neues vom Ontong-Java-Plateau (Westpazifik). *Naturwissenschaften* 79, 541-550.

Butt, F. A., Elverhøi, A., Forsberg, C. F. & Solheim, A. 2001: Evolution of the Scoresby Sund Fan, central East Greenland - Evidence from ODP Site 987. *Norsk Geologisk Tidsskrift* 81, 3-15.

Cathles, L. M., Su, Z. & Chen, D. 2010: The physics of gas chimney and pockmark formation, with implications for assessment of seafloor hazards and gas sequestration. *Marine and Petroleum Geology* 27, 82-91.

Channell, J. E. T., Smelror, M., Jansen, E., Higgins, S. M., Lehman, B., Eidvin, T. & Solheim, A. 1999: Age models for glacial fan deposits off East Greenland and Svalbard (Sites 986 and 987). *Proceedings of the Ocean Drilling Program: Scientific Results* 162, 149-166.

Clausen, L. 1998: The Southeast Greenland glaciated margin: 3D stratal architecture of shelf and deep sea. *Geological Society Special Publication* 129, 173-203.

Døssing, A., Japsen, P., Watts, A. B., Nielsen, T., Jokat, W., Thybo, H. & Dahl-Jensen, T. 2016: Miocene uplift of the NE Greenland margin linked to plate tectonics: Seismic evidence from the Greenland Fracture Zone, NE Atlantic. *Tectonics* 35, 257-282.

Dowdeswell, J. A., Kenyon, N. H. & Laberg, J. S. 1997: The glacier-influenced Scoresby Sund Fan, East Greenland continental margin: Evidence from GLORIA and 3.5 kHz records. *Marine Geology* 143, 207-221.

Ehlers, B.-M. & Jokat, W. 2013: Paleo-bathymetry of the northern North Atlantic and consequences for the opening of the Fram Strait. *Marine Geophysical Research* 34, 25-43.

Engen, Ø., Faleide, J. I. & Dyreng, T. K. 2008: Opening of the Fram Strait gateway: A review of plate tectonic constraints. *Tectonophysics* 450, 51-69.

Evans, J., Dowdeswell, J. A., Grobe, H., Niessen, F., Stein, R., Hubberten, H.-W. & Whittington, R. J. 2002: Late Quaternary sedimentation in Kejser Franz Joseph Fjord and the continental margin of East Greenland. *Geological Society, London, Special Publications* 203, 149-179.

Faugères, J. C., Stow, D. A. V., Imbert, P. & Viana, A. 1999: Seismic features diagnostic of contourite drifts. *Marine Geology* 162, 1-38.

Funder, S., Hjort, C. & Landvik, J. Y. 1994: The last glacial cycles in East Greenland, an overview. *Boreas* 23, 283-293.

Funder, S., Hjort, C., Landvik, J. Y., Nam, S. I., Reeh, N. & Stein, R. 1998: History of a stable ice margin - East Greenland during the middle and upper pleistocene. *Quaternary Science Reviews* 17, 77-123.

García, M., Dowdeswell, J. A., Ercilla, G. & Jakobsson, M. 2012: Recent glacially influenced sedimentary processes on the East Greenland continental slope and deep Greenland Basin. *Quaternary Science Reviews* 49, 64-81.

Håkansson, L., Briner, J., Alexanderson, H., Aldahan, A. & Possnert, G. 2007: 10Be ages from central east Greenland constrain the extent of the Greenland ice sheet during the Last Glacial Maximum. *Quaternary Science Reviews* 26, 2316-2321.

Håvik, L., Pickart, R. S., Våge, K., Torres, D., Thurnherr, A. M., Beszczynska-Möller, A., Walczowski, W. & von Appen, W. J. 2017: Evolution of the East Greenland Current from Fram Strait to Denmark Strait: Synoptic measurements from summer 2012. *Journal of Geophysical Research: Oceans* 122, 1974-1994.

Head, M. J. & Gibbard, P. L. 2005: Early-Middle Pleistocene transitions: An overview and recommendation for the defining boundary. *Geological Society Special Publication* 247, 1-18.

Helmke, J. P., Bauch, H. A., Röhl, U. & Mazaud, A. 2005: Changes in sedimentation patterns of the Nordic seas region across the mid-Pleistocene. *Marine Geology* 215, 107-122.

Henrich, R., Baumann, K. H., Huber, R. & Meggers, H. 2002: Carbonate preservation records of the past 3 Myr in the Norwegian-Greenland Sea and the northern North Atlantic: Implications for the history of NADW production. *Marine Geology* 184, 17-39.

Hopkins, T. S. 1991: The GIN Sea-A synthesis of its physical oceanography and literature review 1972-1985. *Earth Science Reviews* 30, 175-318.

Hubberten, H. W., Grobe, H., Jokat, W., Melles, M., Niessen, F. & Stein, R. 1995: Glacial history of East Greenland explored. *Eos* 76.

Jakobsson, M., Mayer, L., Coakley, B., Dowdeswell, J. A., Forbes, S., Fridman, B., Hodnesdal, H., Noormets, R., Pedersen, R., Rebesco, M., Schenke, H. W., Zarayskaya, Y., Accettella, D., Armstrong, A., Anderson, R. M., Bienhoff, P., Camerlenghi, A., Church, I., Edwards, M., Gardner, J. V., Hall, J. K., Hell, B., Hestvik, O., Kristoffersen, Y., Marcussen, C., Mohammad, R., Mosher, D., Nghiem, S. V., Pedrosa, M. T., Travaglini, P. G. & Weatherall, P. 2012: The International Bathymetric Chart of the Arctic Ocean (IBCAO) Version 3.0. *Geophysical Research Letters* 39, 6.

Jansen, E., Raymo, M. E. & Blum, P. 1996: Proceedings, initial reports, Ocean Drilling Program, Leg 162, North Atlantic-Arctic gateways II. pp. ODP, Texas A and M University, College Station.

Japsen, P., Green, P. F., Bonow, J. M., Nielsen, T. F. D. & Chalmers, J. A. 2014: From volcanic plains to glaciated peaks: Burial, uplift and exhumation history of southern East Greenland after opening of the NE Atlantic. *Global and Planetary Change* 116, 91-114.

Jeansson, E., Jutterström, S., Rudels, B., Anderson, L. G., Anders Olsson, K., Jones, E. P., Smethie, W. M. & Swift, J. H. 2008: Sources to the East Greenland Current and its contribution to the Denmark Strait Overflow. Progress in Oceanography 78, 12-28.

King, E. L., Haflidason, H., Sejrup, H. P. & Løvlie, R. 1998: Glacigenic debris flows on the North Sea Trough Mouth Fan during ice stream maxima. *Marine Geology* 152, 217-246.

King, E. L., Sejrup, H. P., Haflidason, H., Elverhøi, A. & Aarseth, I. 1996: Quaternary seismic stratigraphy of the North Sea Fan: Glaciallyfed gravity flow aprons, hemipelagic sediments, and large submarine slides. *Marine Geology* 130, 293-315.

Knutz, P. C., Hopper, J. R., Gregersen, U., Nielsen, T. & Japsen, P. 2015: A contourite drift system on the Baffin Bay–West Greenland margin linking Pliocene Arctic warming to poleward ocean circulation. *Geology* 43, 907-910.

Laberg, J. S., Forwick, M., Husum, K. & Nielsen, T. 2013: A re-evaluation of the Pleistocene behavior of the Scoresby Sund sector of the Greenland Ice Sheet. *Geology* 41, 1231-1234.

Laberg, J. S., Rydningen, T. A., Forwick, M. & Husum, K. 2017: Depositional processes on the distal Scoresby Trough Mouth Fan (ODP Site 987): Implications for the Pleistocene evolution of the Scoresby Sund Sector of the Greenland Ice Sheet. *Marine Geology*.

Laberg, J. S. & Vorren, T. O. 1995: Late Weichselian submarine debris flow deposits on the Bear Island Trough Mouth Fan. *Marine Geology* 127, 45-72.

Larsen, H. C., Saunders, A. D., Clift, P. D., Ali, J., Begét, J., Cambray, H., Demant, A., Fitton, G., Fram, M. S., Fukuma, K., Gieskes, J., Holmes, M. A., Hunt, J., Lacasse, C., Larsen, L. M., Lykke-Anderson, H., Meltser, A., Morrison, M. L., Nemoto, N., Okay, N., Saito, S., Sinton, C., Spezzaferri, S., Stax, R., Vallier, T. L., Vandamme, D., Wei, W. & Werner, R. 1994: Seven million years of glaciation in Greenland. *Science* 264, 952-955.

Marchitto Jr, T. M., Oppo, D. W. & Curry, W. B. 2002: Paired benthic foraminiferal Cd/Ca and Zn/Ca evidence for a greatly increased presence of Southern Ocean Water in the glacial North Atlantic. *Paleoceanography* 17, 10-11.

Mattingsdal, R., Knies, J., Andreassen, K., Fabian, K., Husum, K., Grøsfjeld, K. & De Schepper, S. 2014: A new 6Myr stratigraphic framework for the Atlantic-Arctic Gateway. *Quaternary Science Reviews* 92, 170-178.

Migeon, S., Cattaneo, A., Hassoun, V., Larroque, C., Corradi, N., Fanucci, F., Dano, A., de Lepinay, B. M., Sage, F. & Gorini, C. 2011: Morphology, distribution and origin of recent submarine landslides of the Ligurian Margin (North-western Mediterranean): Some insights into geohazard assessment. *Marine Geophysical Research* 32, 225-243.

Mokeddem, Z. & McManus, J. F. 2016: Persistent climatic and oceanographic oscillations in the subpolar North Atlantic during the MIS 6 glaciation and MIS 5 interglacial. *Paleoceanography* 31, 758-778.

Mulder, T., Faugères, J. C. & Gonthier, E. 2008: Chapter 21 Mixed Turbidite-Contourite Systems. In Rebesco, M. & Camerlenghi, A. (eds.): *Developments in Sedimentology* 60, 435-456.

Nelson, C. H., Escutia, C., Damuth, J. E. & Twichell, D. C. 2011: Interplay of mass-transport and turbidite-system deposits in different active tectonic and passive continental margin settings: external and local controlling factors. In Shipp, R. C., Weimer, P. & Posamentier, H. W. (eds.): *Mass-transport Deposits in Deepwater Settings*, 39-66 pp. SEPM (Society for Sedimentary Geology).

Nielsen, T., De Santis, L., Dahlgren, K. I. T., Kuijpers, A., Laberg, J. S., Nygård, A., Praeg, D. & Stoker, M. S. 2005: A comparison of the NW European glaciated margin with other glaciated margins. *Marine and Petroleum Geology* 22, 1149-1183.

Nielsen, T. & Kuijpers, A. 2013: Only 5 southern Greenland shelf edge glaciations since the early Pliocene. *Sci Rep* 3, 1875.

Nygard, A., Sejrup, H. P., Haflidason, H. & King, E. L. 2002: Geometry and genesis of glacigenic debris flows on the North Sea Fan: TOBI imagery and deep-tow boomer evidence. *Marine Geology* 188, 15-33.

Ó Cofaigh, C., Dowdeswell, J. A., Evans, J., Kenyon, N. H., Taylor, J., Mienert, J. & Wilken, M. 2004: Timing and significance of glacially influenced mass-wasting in the submarine channels of the Greenland Basin. *Marine Geology* 207, 39-54.

Ó Cofaigh, C., Taylor, J., Dowdeswell, J. A. & Pudsey, C. J. 2003: Palaeo-ice streams, trough mouth fans and high-latitude continental slope sedimentation. *Boreas* 32, 37-55.

Ó Cofaigh, C., Taylor, J., Dowdeswell, J. A., Rosell-Melé, A., Kenyon, N. H., Evans, J. & Mienert, J. 2002: Sediment reworking on high-latitude continental margins and its implications for palaeoceanographic studies: Insights from the Norwegian-Greenland Sea. *Geological Society Special Publication* 203, 325-348.

Parnell-Turner, R., White, N. J., McCave, I. N., Henstock, T. J., Murton, B. & Jones, S. M. 2015: Architecture of North Atlantic contourite drifts modified by transient circulation of the Icelandic mantle plume. *Geochemistry, Geophysics, Geosystems* 16, 3414-3435.

Payton, C. E. 1977: Seismic Stratigraphy-Applications to Hydrocarbon Exploration. pp., Tulsa, Okla.

Pérez, L. F., Nielsen, T., Knutz, P. C., Kuijpers, A. & Damm, V. 2017: Large-scale evolution of the central-east Greenland margin: New insights to the North Atlantic glaciation history. *Global and Planetary Change*.

Pickering, K. T. & Hiscot, R. N. 2016: Deep Marine Systems. Processes, Deposits, Environments, Tectonics and Sedimentation. In Wiley, A. (ed.). AGU & Wiley, Oxford.

Poore, H. R., Samworth, R., White, N. J., Jones, S. M. & McCave, I. N. 2006: Neogene overflow of Northern Component Water at the Greenland-Scotland Ridge. *Geochemistry, Geophysics, Geosystems* 7, n/a-n/a.

Pudsey, C. J. & Camerlenghi, A. 1998: Glacial-interglacial deposition on a sediment drift on the Pacific margin of the Antarctic Peninsula. Antarctic Science 10, 286-308.

Raymo, M. E., Oppo, D. W. & Curry, W. 1997: The Mid-Pleistocene climate transition: A deep sea carbon isotopic perspective. *Paleoceanography* 12, 546-559.

Raymo, M. E., Oppo, D. W., Flower, B. P., Hodell, D. A., McManus, J. F., Venz, K. A., Kleiven, K. F. & McIntyre, K. 2004: Stability of North Atlantic water masses in face of pronounced climate variability during the Pleistocene. *Paleoceanography* 19, n/a-n/a.

Reading, H. G. 1996: Sedimentary Environments. Processes, Facies and Stratigraphy. 3 ed. Blackwell Science.

Rebesco, M. 2005: Contourites. In Richard, C., Selley, R. C., Cocks, L. R. M. & Plimer, I. R. (eds.): *Encyclopedia of Geology*, 513-527 pp. Elsevier, London.

Rebesco, M., Hernández-Molina, F. J., Van Rooij, D. & Wåhlin, A. 2014: Contourites and associated sediments controlled by deep-water circulation processes: state of the art and future considerations. *Marine Geology* 352, 111-154.

Sarnthein, M., Bartoli, G., Prange, M., Schmittner, A., Schneider, B., Weinelt, M., Andersen, N. & Garbe-Schönberg, D. 2009: Mid-Pliocene shifts in ocean overturning circulation and the onset of Quaternary-style climates. *Climate of the Past Discussions* 5, 269-283.

Solheim, A., Faleide, J. I., Andersen, E. S., Elverhøi, A., Forsberg, C. F., Vanneste, K., Uenzelmann-Neben, G. & Channell, J. E. T. 1998: Late cenozoic seismic stratigraphy and glacial geological development of the East Greenland and Svalbard-Barents sea continental margins. *Quaternary Science Reviews* 17, 155-184.

Stein, R., Grobe, H., Hubberten, H., Marienfeld, P. & Nam, S. 1993: Latest Pleistocene to Holocene changes in glaciomarine sedimentation in Scoresby Sund and along the adjacent East Greenland Continental Margin: Preliminary results. *Geo-Marine Letters* 13, 9-16.

Stein, R., Nam, S. I., Grobe, H. & Hubberten, H. 1996: Late Quaternary glacial history and short-term ice-rafted debris fluctuations along the East Greenland continental margin. *Geological Society Special Publication* 111, 135-151.

Stokes, C. R., Margold, M., Clark, C. D. & Tarasov, L. 2016: Ice stream activity scaled to ice sheet volume during Laurentide Ice Sheet deglaciation. *Nature* 530, 322-326.

Stow, D. A. V., Faugeres, J. C., Howe, J. A., Pudsey, C. J. & Viana, A. R. 2002: Bottom currents, contourites and deep sea sediment drifts: current state-of-the-art. 7-20 pp. *Geological Society of London Memories* 22, 7-20.

Swift, D. A., Persano, C., Stuart, F. M., Gallagher, K. & Whitham, A. 2007: A reassessment of the role of ice sheet glaciation in the long-term evolution of the East Greenland fjord region. *Geomorphology* 97, 109-125.

Thiede, J., Jessen, C., Knutz, P., Kuijpers, A., Mikkelsen, N., Nørgaard-Pedersen, N. & Spielhagen, R. F. 2010: Millions of years of Greenland ice sheet history recorded in Ocean sediments. *Polarforschung* 80, 141-159.

Tripati, A. K., Eagle, R. A., Morton, A., Dowdeswell, J. A., Atkinson, K. L., Bahé, Y., Dawber, C. F., Khadun, E., Shaw, R. M. H., Shorttle, O. & Thanabalasundaram, L.

2008: Evidence for glaciation in the Northern Hemisphere back to 44 Ma from ice-rafted debris in the Greenland Sea. *Earth and Planetary Science Letters* 265, 112-122.

Våge, K., Pickart, R. S., Spall, M. A., Moore, G. W. K., Valdimarsson, H., Torres, D. J., Erofeeva, S. Y. & Nilsen, J. E. Ø. 2013: Revised circulation scheme north of the Denmark Strait. *Deep Sea Research Part I: Oceanographic Research Papers* 79, 20-39.

Vanneste, K., Uenzelmann-Neben, G. & Miller, H. 1995: Seismic evidence for long-term history of glaciation on central East Greenland shelf south of Scoresby Sund. *Geo-Marine Letters* 15, 63-70.

Vorren, T. O. & Laberg, J. S. 1997: Trough mouth fans - Palaeoclimate and ice-sheet monitors. *Quaternary Science Reviews* 16, 865-881.

Wilken, M. & Mienert, J. 2006: Submarine glacigenic debris flows, deep-sea channels and past ice-stream behaviour of the East Greenland continental margin. *Quaternary Science Reviews* 25, 784-810.

Wolf, T. C. W. & Thiede, J. 1991: History of terrigenous sedimentation during the past 10 m.y. in the North Atlantic (ODP Legs 104 and 105 and DSDP Leg 81). Marine *Geology* 101, 83-102.

Wright, A. K. & Flower, B. P. 2002: Surface and deep ocean circulation in the subpolar North Atlantic during the mid-Pleistocene revolution. *Paleoceanography* 17, 20-21-20-16.

Wright, J. D. & Miller, K. G. 1996: Control of North Atlantic Deep Water Circulation by the Greenland-Scotland Ridge. *Paleoceanography* 11, 157-170.

Wynn, R. B. & Stow, D. A. V. 2002: Classification and characterisation of deep-water sediment waves. *Marine Geology* 192, 7-22.

Zachos, J. C., Dickens, G. R. & Zeebe, R. E. 2008: An early Cenozoic perspective on greenhouse warming and carbon-cycle dynamics. *Nature* 451, 279-283.

Zhuravleva, A., Bauch, H. A. & Van Nieuwenhove, N. 2017: Last Interglacial (MIS5e) hydrographic shifts linked to meltwater discharges from the East Greenland margin. *Quaternary Science Reviews* 164, 95-109.

Figure captions

Figure 1.- Regional setting of the study area. A) Oceanographic framework of the North Atlantic Ocean based on Wolf and Thiede (1991) and Våge et al. (2013). Major boundary currents are represented, distinguishing between warm (red) and cold (blue) flows: AT, Arctic Throughflow; EGC, East Greenland Current; GSDW, Greenland Sea Deep Water; NAC, Norwegian Atlantic Current; and Deep Western Boundary Current (DWBC) and North Icelandic Irminger Current (NIIC) as part of the Atlantic Meridional Overturning Circulation (AMOC). B) Bathymetric map of the study area based on the International Bathymetric Chart of the Arctic Ocean (IBCAO, Jacobsson et al., 2012). Isobaths every 500 m. Location of the data used in this work: Red lines, tracks of the chirp sub-bottom profiles; Black lines, single-channel seismic profiles (Notice the location of profiles CAGEAO13_034 (034) and CAGE_OA2013-032 (032) shown in figures 7 and 8 respectively). The white squares mark the location of the seismic sections shown in Fig. 3 of profile CAGE_OA2013-032 and profiles GGU82-12 and 11HH-GEO8144-022 south of the study area tie with ODP 987 (red dot) in the age model (Perez et al., 2017), the location multi-channel seismic profiles connecting both areas is shown in grey. The seismic correlation from the study area to the ODP 987 shown in Fig. 2 is marked in green as profile A-B. The location of the gravity cores available in the study area is shown as purple dots.

Figure 2.- Seismic correlation between the study area off Liverpool Land, and the ODP 987 off Scoresby Sund. Discontinuities a, b and c (D-a, D-b, D-c, respectively) are marked. Vertical scale in two-way-travel-time (TWTT). The location of the composite line is shown in Fig. 1 as profile A-B.

Figure 3.- Minor discontinuities (doted black lines) in line CAGE_OA2013-032 correlated with the lines GGU82-12 and 11HH-GEO8144-022 tie to ODP 987 off Scoresby Sund (for locations, see Fig. 1). Vertical scale in two-way-travel-time (TWTT). D-a and D-b (black lines) correspond with the discontinuities described in Pérez et al. (2018), and R1 (doted black line) corresponds with the local upper discontinuity identified in Channell et al. (1999) and Jansen et al. (1996) in the ODP site 987. Ages in Ma.

Figure 4.- Magnetic susceptibility curve of gravity core HH13-099GC (1550 m water depth) compared to the calibrated magnetic susceptibility curve of HH13-092GC (1595 m water depth) and correlated with the Marine Isotope Stages (MIS). Cal years, Calibrated ^{14}C years; LGM, Last Glacial Maximum. Note the location of 46.8 cal ka age at 2.05 m deep discussed in the text. Location of the cores HH92 and HH99 in Fig. 1.

Figure 5.- Seafloor features in the study area. A) Swath bathymetry map 30 x 30 m cell grid overlaying the International Bathymetric Chart of the Arctic Ocean (IBCAO, Jacobsson et al., 2012) bathymetry, with black isobaths every 500 m and blue isobaths every 100 m. Note the zoom over the pockmarks and the seafloor profile over the sediment waves in the northern (i) and southern (ii) part of the study area. B) Swath bathymetry data of the study area in a oblique view.

Figure 6.- Sub-bottom features. A) Chirp sub-bottom profile across the northern study area, see location in b. Notice the plastered and mounded drifts in the basinal area. Zoom over the mounded drift in the square. B) Distribution of the main features

identified in the chirp sub-bottom profiles which location is marked by the grey lines. Location of the chirp sub-bottom profiles in Fig. 6a, 7a and 8a is shown. The purple and pink doted lines show the distribution of the chirp units c2 and c1 respectively, thickness in ms two-way-travel-time (TWTT).

Figure 7.- Profile CAGE_OA2013-034 along the lower slope of the study area. See location in Fig. 1 and 6. A) Chirp sub-bottom profile. The main identified features are pointed. Detail of the chirp unit in the square. B) High-resolution single-channel seismic profile: seismic signal (top) and interpretation (bottom). Discontinuities a and b are in red and minor discontinuities in orange. Distinguished mass transport deposit (MTD) bodies of SU2 are shadow in different colours. The location of the gravity core HH2013_99GC is shown. TWTT; two-way-travel-time.

Figure 8.- Profile CAGE_OA2013-032 along the base of the slope of the study area. See location in Fig. 1 and 6. A) Chirp sub-bottom profile. The main identified features are pointed. Zoom over smooth wavy features in the square. B) High-resolution single-channel seismic profile: seismic signal (top) and interpretation (bottom). Discontinuities a and b are in red and minor discontinuities in orange. Distinguished mass transport deposit (MTD) bodies of SU2 are shadow in different colours. TWTT; two-way-travel-time.

Figure 9.- Regional map where the major depocentres of the units (A) and subunits (B) are highlighted. Note that the lines represent the boundary of the depocentres.

Figure 10.- Location of the major mass transport deposits (MTDs) identified in the sedimentary record as distinguished in the seismic profiles. The different MTD bodies distinguished in SU2 have been highlighted in different colours following Fig. 7 and 8.

Figure 11.- 3D sketch of the central-east Greenland margin off Liverpool Land showing the main morphological features and dominating sedimentary processes.

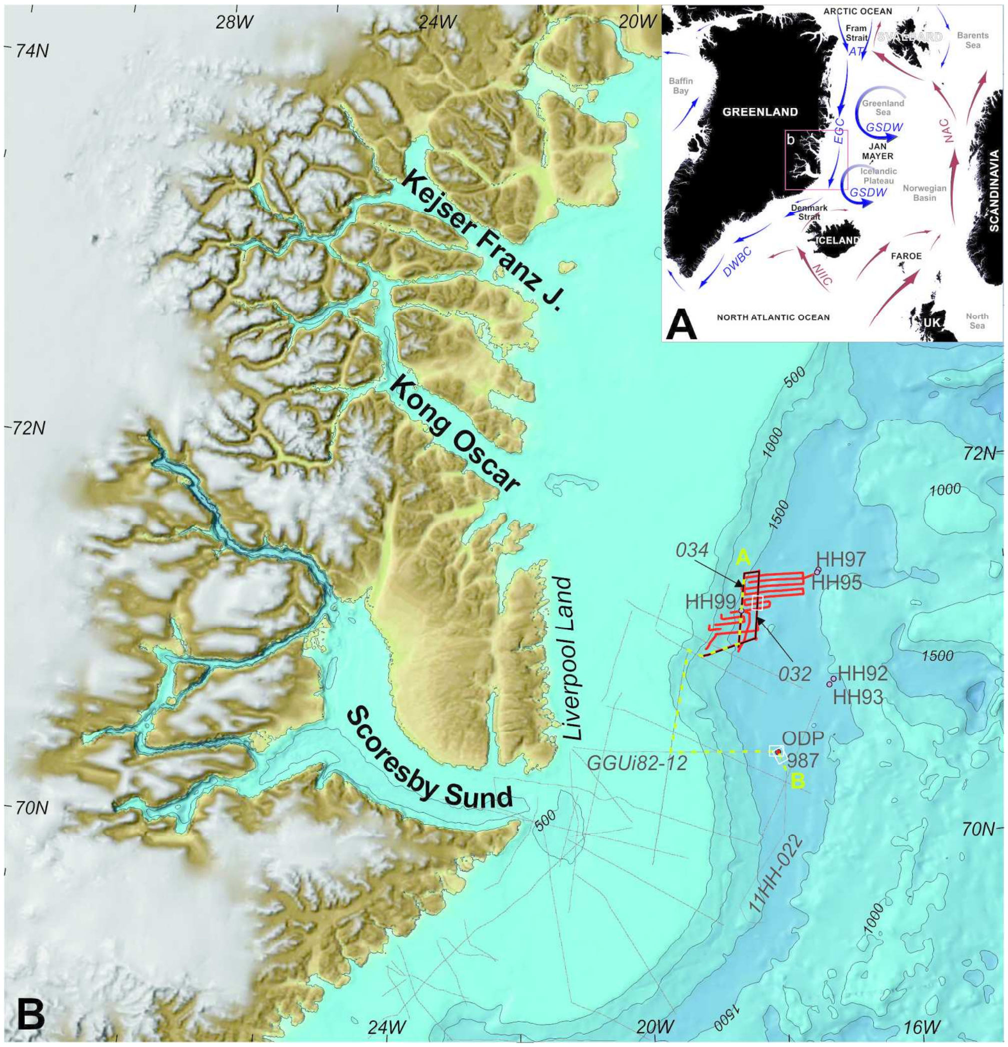

Figure 1.- Regional setting of the study area. A) Oceanographic framework of the North Atlantic Ocean based on Wolf and Thiede (1991) and Våge et al. (2013). Major boundary currents are represented, distinguishing between warm (red) and cold (blue) flows: AT, Arctic Throughflow; EGC, East Greenland Current; GSDW, Greenland Sea Deep Water; NAC, Norwegian Atlantic Current; and Deep Western Boundary Current (DWBC) and North Icelandic Irminger Current (NIIC) as part of the Atlantic Meridional Overturning Circulation (AMOC). B) Bathymetric map of the study area based on the International Bathymetric Chart of the Arctic Ocean (IBCAO, Jacobsson et al., 2012). Isobaths every 500 m. Location of the data used in this work: Red lines, tracks of the chirp sub-bottom profiles; Black lines, single-channel seismic profiles (Notice the location of profiles CAGEAO13_034 (034) and CAGE_OA2013-032 (032) shown in figures 7 and 8 respectively). The white squares mark the location of the seismic sections shown in Fig. 3 of profile CAGE_OA2013-032 and profiles GGU82-12 and 11HH-GEO8144-022 south of the study area tie with ODP 987 (red dot) in the age model (Perez et al., 2017), the location multi-channel seismic profiles connecting both areas is shown in grey. The seismic correlation from the study area to the ODP 987 shown in Fig. 2 is marked in green as profile A-B. The location of the gravity cores available in the study area is shown as purple dots.

195x202mm (300 x 300 DPI)

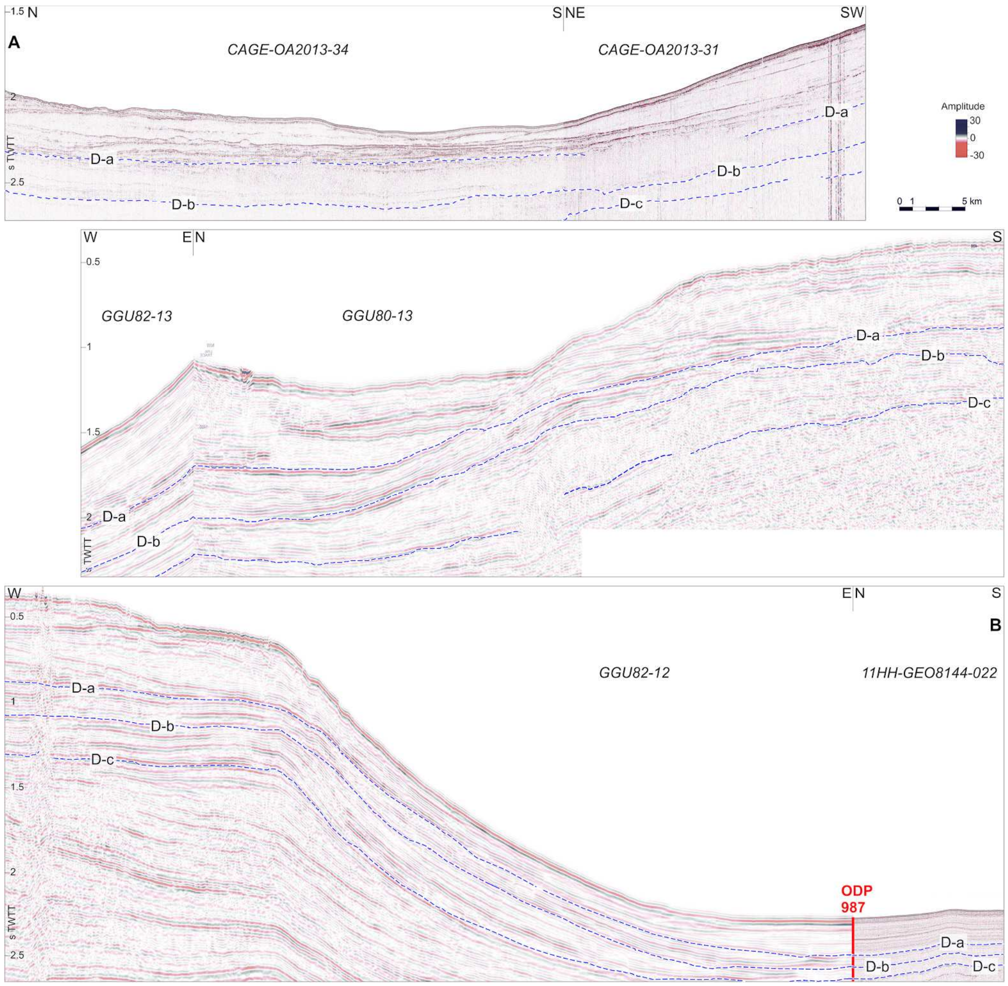

Figure 2.- Seismic correlation between the study area off Liverpool Land, and the ODP 987 off Scoresby Sund. Discontinuities a, b and c (D-a, D-b, D-c, respectively) are marked. Vertical scale in two-way-travel-time (TWTT). The location of the composite line is shown in Fig. 1 as profile A-B.

209x204mm (300 x 300 DPI)

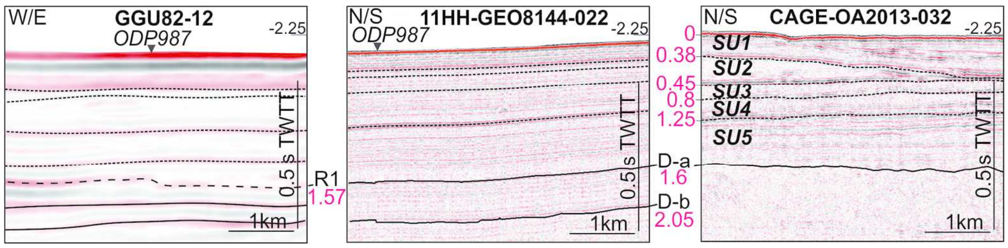

Figure 3.- Minor discontinuities (doted black lines) in line CAGE_OA2013-032 correlated with the lines GGU82-12 and 11HH-GEO8144-022 tie to ODP 987 off Scoresby Sund (for locations, see Fig. 1). Vertical scale in two-way-travel-time (TWTT). D-a and D-b (black lines) correspond with the discontinuities described in Pérez et al. (2018), and R1 (doted black line) corresponds with the local upper discontinuity identified in Channell et al. (1999) and Jansen et al. (1996) in the ODP site 987. Ages in Ma.

173x41mm (300 x 300 DPI)

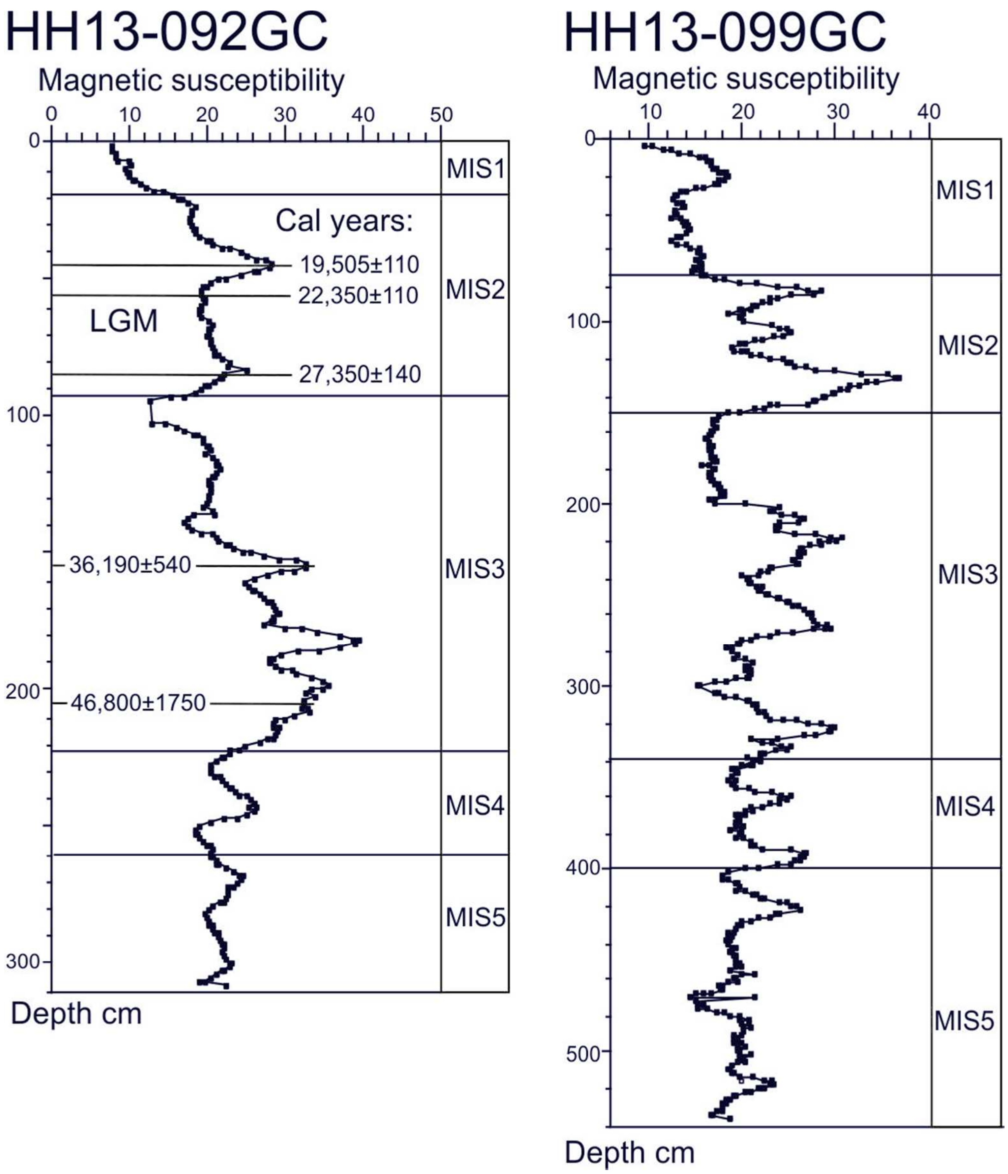

Figure 4.- Magnetic susceptibility curve of gravity core HH13-099GC (1550 m water depth) compared to the calibrated magnetic susceptibility curve of HH13-092GC (1595 m water depth) and correlated with the Marine Isotope Stages (MIS). Cal years, Calibrated 14C years; LGM, Last Glacial Maximum. Note the location of 46.8 cal ka age at 2.05 m deep discussed in the text. Location of the cores HH92 and HH99 in Fig. 1.

92x106mm (300 x 300 DPI)

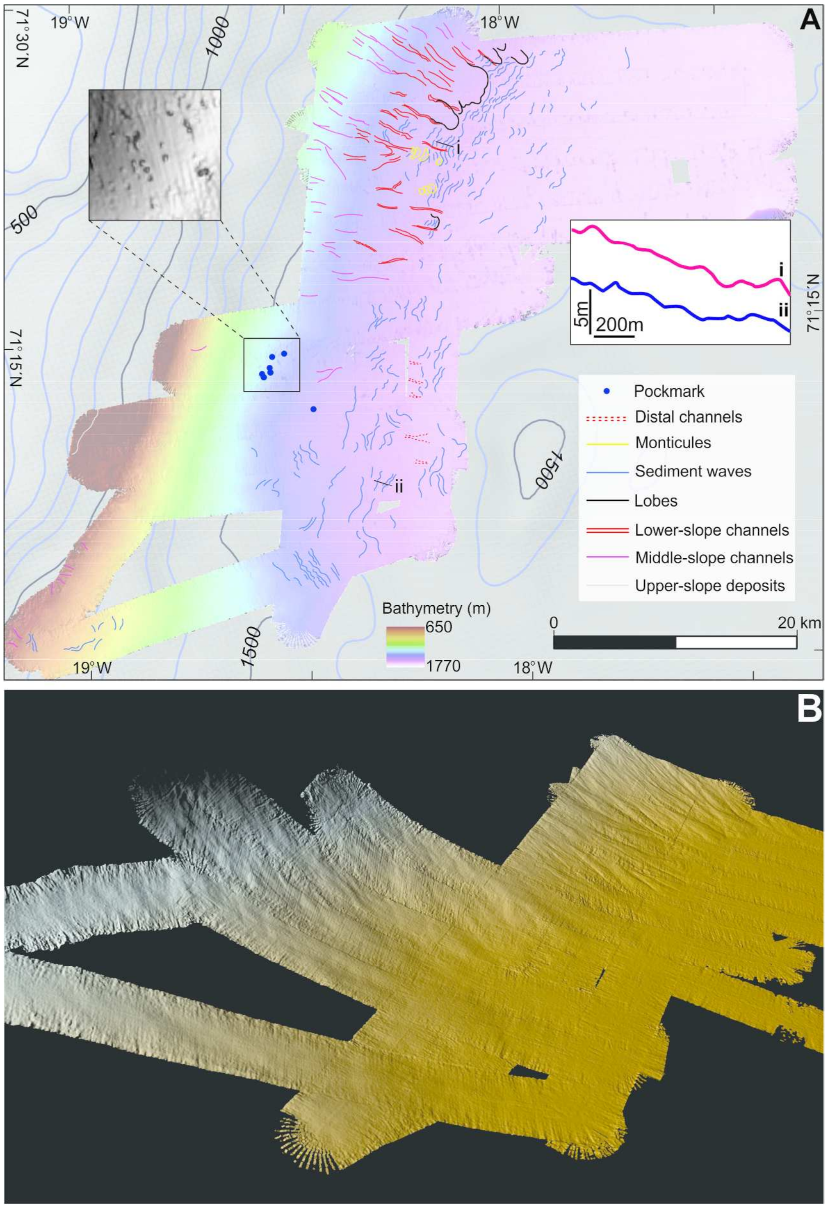

Figure 5.- Seafloor features in the study area. A) Swath bathymetry map 30 x 30 m cell grid overlaying the International Bathymetric Chart of the Arctic Ocean (IBCAO, Jacobsson et al., 2012) bathymetry, with black isobaths every 500 m and blue isobaths every 100 m. Note the zoom over the pockmarks and the seafloor profile over the sediment waves in the northern (i) and southern (ii) part of the study area. B) Swath bathymetry data of the study area in oblique view.

182x266mm (300 x 300 DPI)

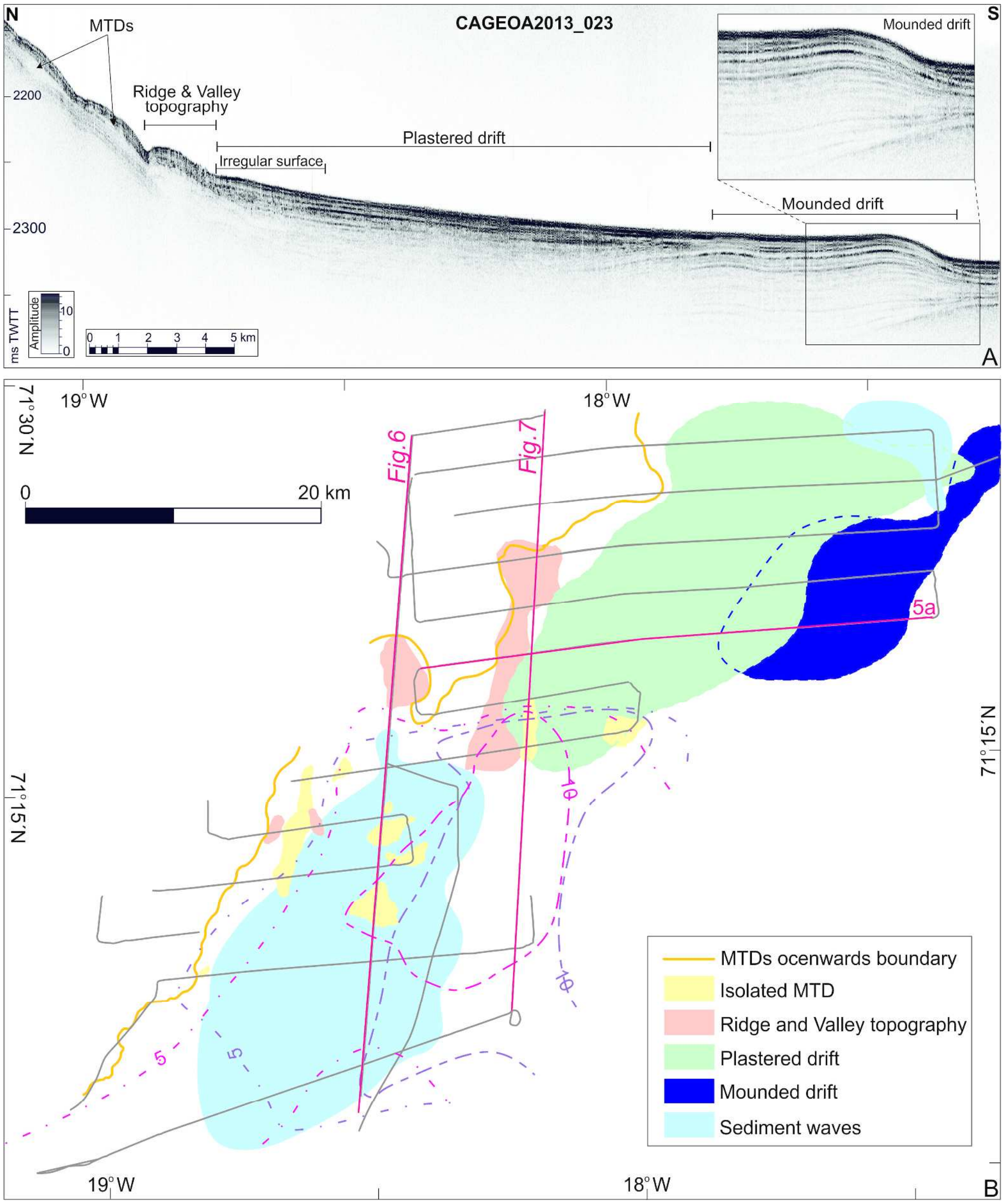

Figure 6.- Sub-bottom features. A) Chirp sub-bottom profile across the northern study area, see location in b. Notice the plastered and mounded drifts in the basinal area. Zoom over the mounded drift in the square. B) Distribution of the main features identified in the chirp sub-bottom profiles which location is marked by the grey lines. Location of the chirp sub-bottom profiles in Fig. 6a, 7a and 8a is shown. The purple and pink doted lines show the distribution of the chirp units c2 and c1 respectively, thickness in ms two-way-travel-time (TWTT).

296x355mm (300 x 300 DPI)

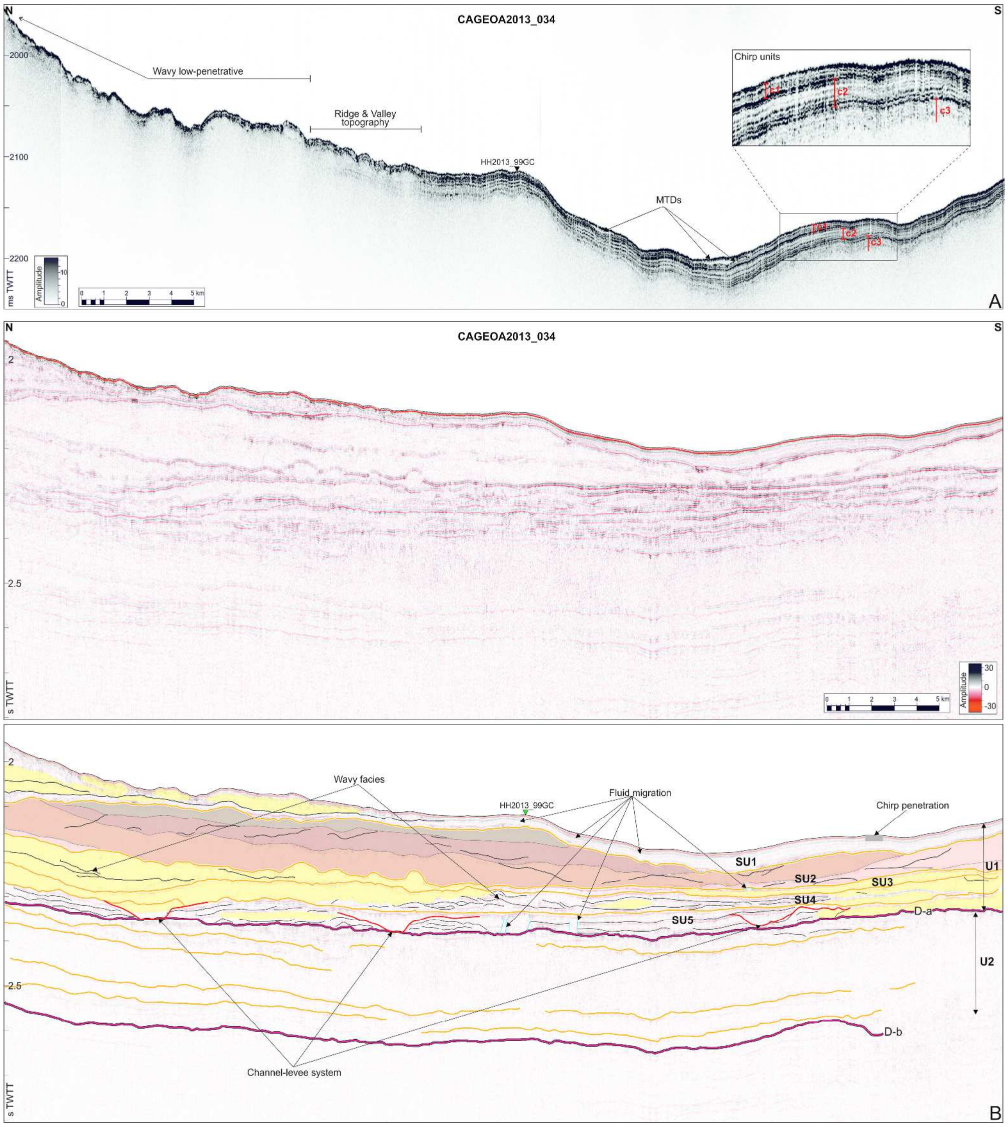

Figure 7.- Profile CAGE_OA2013-034 along the lower slope of the study area. See location in Fig. 1 and 6. A) Chirp sub-bottom profile. The main identified features are pointed. Detail of the chirp unit in the square. B) High-resolution single-channel seismic profile: seismic signal (top) and interpretation (bottom). Discontinuities a and b are in red and minor discontinuities in orange. Distinguished mass transport deposit (MTD) bodies of SU2 are shadow in different colours. The location of the gravity core HH2013_99GC is shown. TWTT; two-way-travel-time.

447x499mm (300 x 300 DPI)

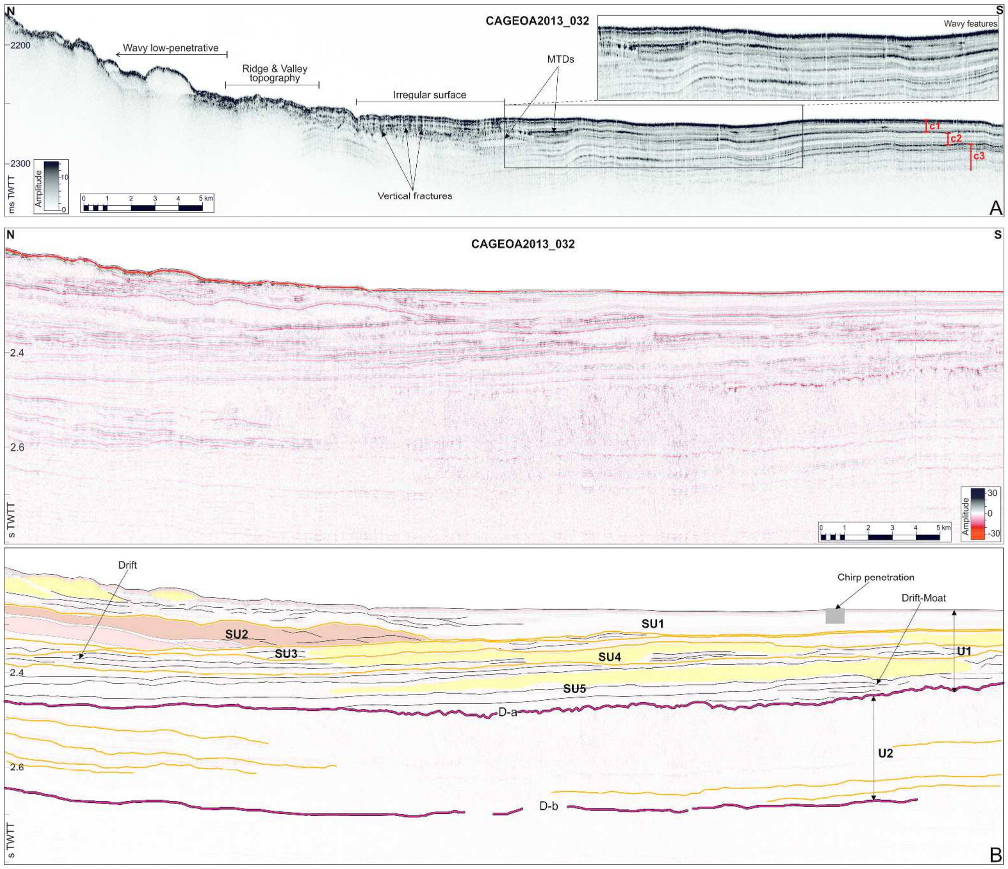

Figure 8.- Profile CAGE_OA2013-032 along the base of the slope of the study area. See location in Fig. 1 and 6. A) Chirp sub-bottom profile. The main identified features are pointed. Zoom over smooth wavy features in the square. B) High-resolution single-channel seismic profile: seismic signal (top) and interpretation (bottom). Discontinuities a and b are in red and minor discontinuities in orange. Distinguished mass transport deposit (MTD) bodies of SU2 are shadow in different colours. TWTT; two-way-travel-time.

422x363mm (300 x 300 DPI)

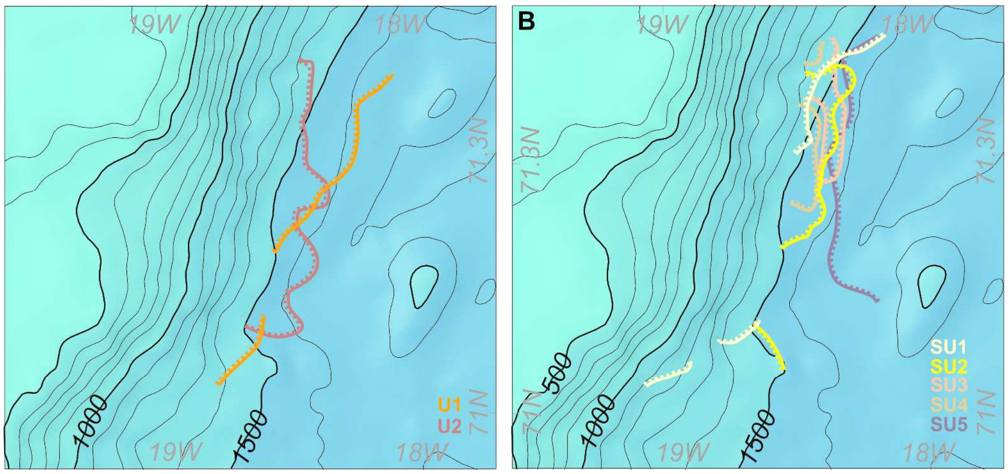

Figure 9.- Regional map where the major depocentres of the units (A) and subunits (B) are highlighted. Note that the lines represent the boundary of the depocentres.

328x153mm (300 x 300 DPI)

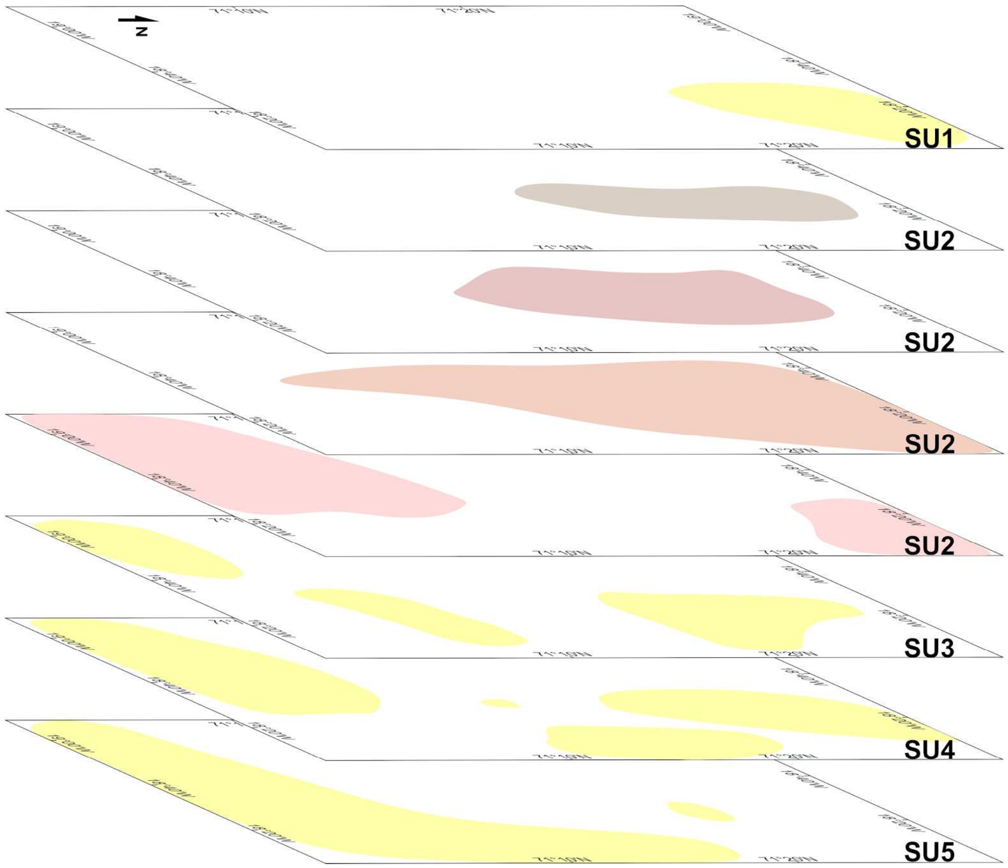

Figure 10.- Location of the major mass transport deposits (MTDs) identified in the sedimentary record as distinguished in the seismic profiles. The different MTD bodies distinguished in SU2 have been highlighted in different colours following Fig. 7 and 8.

189x163mm (300 x 300 DPI)

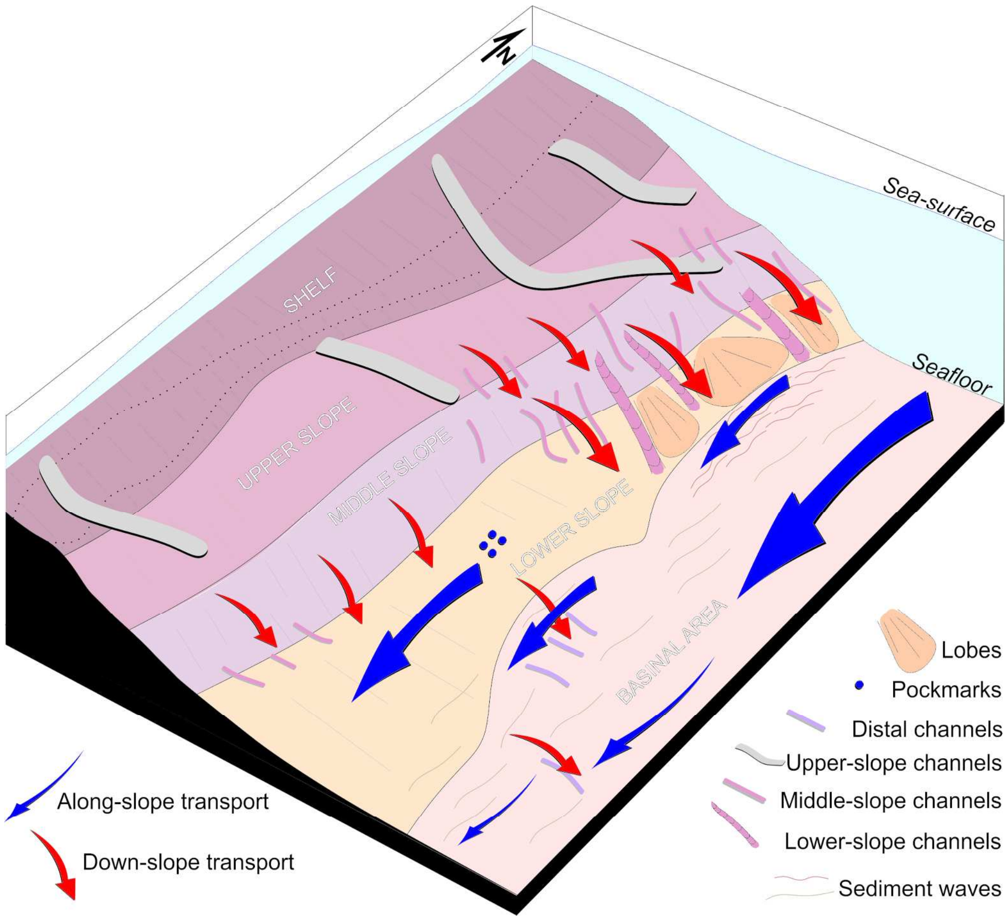

Figure 11.- 3D sketch of the central-east Greenland margin off Liverpool Land showing the main morphological features and dominating sedimentary processes.

189x173mm (300 x 300 DPI)